Article:
Hadjisolomou, P., Jeong, T. M., Kolenaty, D. et al. (2023) Gamma-flash generation in multi-petawatt laser-matter interactions. Physics of Plasmas. 093103. ISSN: 1089-7674

https://doi.org/10.1063/5.0158264

RESEARCH ARTICLE | SEPTEMBER 11 2023

Gamma-flash generation in multi-petawatt laser–matter interactions

Special Collection: Relativistic Plasma in Supercritical Electromagnetic Fields

P. Hadjisolomou ; T. M. Jeong; D. Kolenaty ; A. J. Macleod ; V. Olšovcová ; R. Versaci ; C. P. Ridgers ; S. V. Bulanov

Phys. Plasmas 30, 093103 (2023)
https://doi.org/10.1063/5.0158264

Gamma-flash generation in multi-petawatt laser–matter interactions

Cite as: Phys. Plasmas **30**, 093103 (2023); doi: 10.1063/5.0158264
Submitted: 16 May 2023 · Accepted: 15 August 2023 ·
Published Online: 11 September 2023

P. Hadjisolomou,[1,a)] T. M. Jeong,[1] D. Kolenaty,[2] A. J. Macleod,[1] V. Olšovcová,[1] R. Versaci,[1] C. P. Ridgers,[3] and S. V. Bulanov[1,b)]

AFFILIATIONS

[1]ELI Beamlines Facility, Extreme Light Infrastructure ERIC, Za Radnicí 835, 25241 Dolní Břežany, Czech Republic
[2]Department of Physics and NTIS–European Centre of Excellence, University of West Bohemia, Univerzitní 8, 306 14 Plzeň, Czech Republic
[3]York Plasma Institute, Department of Physics, University of York, Heslington, York, North Yorkshire YO10 5DD, United Kingdom

Note: This paper is part of the Special Topic: Relativistic Plasma in Supercritical Electromagnetic Fields.
[a)]**Author to whom correspondence should be addressed:** Prokopis.Hadjisolomou@eli-beams.eu
[b)]**Also at:** National Institutes for Quantum and Radiological Science and Technology (QST), Kansai Photon Science Institute, 8-1-7 Umemidai, Kizugawa, Kyoto 619-0215, Japan

ABSTRACT

The progressive development of high power lasers over the last several decades enables the study of γ-photon generation when an intense laser beam interacts with matter, mainly via inverse Compton scattering at the high intensity limit. γ-ray flashes are a phenomenon of broad interest, drawing the attention of researchers working in topics ranging from cosmological scales to elementary particle scales. Over the last few years, a plethora of studies predict extremely high laser energy to γ-photon energy conversion using various target and/or laser field configurations. The aim of this article is to discuss several recently proposed γ-ray flash generation schemes, as a guide for upcoming γ-photon related experiments and for further evolution of the presently available theoretical schemes.

I. INTRODUCTION

Development of multi-PW lasers[1–4] paves the path toward the possibility of the experimental investigation of the radiation dominated regime where radiation reaction and quantum effects play a significant role in particle dynamics. Today, laser power of 10 PW has been reported,[1] whilst laser intensity exceeding 10^{23} Wcm^{-2} has been reached.[2]

Intense laser–solid interactions result in several distinct populations of energetic γ-photons, leptons (electrons, positrons), and hadrons (protons, ions). For clarity, we refer to γ-photons as high energy (above 1 MeV) photons, not to photons that originate from the nucleus. Under the effect of strong fields electrons and positrons quickly become relativistic due to their relatively low mass. As the electric field is not a Lorentz invariant, electrons in their boosted frame can approach or even surpass the Schwinger field,[5,6] E_S, at which spontaneous electron–positron (e^-e^+) pair generation can occur due to vacuum breakdown. Therefore, QED effects can be observed even with currently available lasers.

Although particle-in-cell (PIC) codes were developed many decades ago, QED PIC routines have been developed for major PIC codes only in the last decade. These routines allow extensive computational investigation of the collective behavior governing QED effects in a multi-species plasma which is inevitably generated when a strong laser field interacts with matter. Two main processes dominate at ultrahigh intensities and are implemented in the QED PIC codes, being the emission of a γ-photon through multiphoton (inverse) Compton scattering[7–10] and the generation of an e^-e^+ pair through the multiphoton Breit–Wheeler[7,11–13] process.

Here, we focus on Compton γ-photon emission. Bright γ-photon sources find applications in a plethora of topics, including but not limited to study of fundamental physics,[14] positron generation,[15–17] neutron sources[18] astrophysical studies,[16,19] photonuclear fission,[20,21] radiotherapy,[22] fine measurement of atomic nuclei,[23] and shock-wave studies.[24,25]

II. QED PROCESSES IN STRONG FIELDS

A. Strong field parameters

The interaction of an electromagnetic field with charged particles is conveniently parametrized by the normalized dimensionless electromagnetic wave amplitude,[26]

$$a_0 = \frac{eE_0}{m_e \omega_l c}. \tag{1}$$

Here, e is the elementary charge, E_0 is the electric field amplitude, m_e is the electron rest mass, c is the speed of light in vacuum, and $\omega_l = 2\pi c/\lambda_l$ is the laser frequency (wavelength λ_l). When $a_0 = 1$, the work done by electric field E_0 acting on a particle of charge e over a distance of $\lambda_l/(2\pi)$, equals $m_e c^2$. An electron oscillating in the laser field is considered as relativistic when $a_0 \geqslant 1$, since then the electron obtains velocities similar to c during its oscillatory motion. For a laser with linear polarization, a_0 is related to the relativistic electron Lorentz factor as $\gamma_e = \sqrt{1 + a_0^2/2}$, while for a laser with circular polarization it is related as $\gamma_e = \sqrt{1 + a_0^2}$. The laser intensity is connected to a_0 by

$$I_L = \frac{\varepsilon_0 \omega_l^2 c^3 a_0^2}{2e^2} \approx 1.37 \times 10^{18} \left(\frac{1\,\mu\text{m}}{\lambda_l}\right)^2 a_0^2 \ \text{Wcm}^{-2}, \tag{2}$$

where ε_0 is the vacuum permittivity.

A dimensionless parameter describing the radiation losses is

$$\varepsilon_{rad} = \frac{4\pi r_e}{3\lambda_l}, \tag{3}$$

where $r_e = e^2/(4\pi\varepsilon_0 m_e c^2)$ is the classical electron radius. The radiation reaction refers to the recoil force experienced by an accelerated particle emitting radiation.

The relativistic gauge invariant parameter for electron is χ_e,

$$\chi_e = \sqrt{\left(\gamma_e \frac{\boldsymbol{E}}{E_S} + \frac{\boldsymbol{p}}{m_e} \times \frac{\boldsymbol{B}}{E_S}\right)^2 - \left(\frac{\boldsymbol{p}}{m_e c} \cdot \frac{\boldsymbol{E}}{E_S}\right)^2}, \tag{4}$$

and it characterizes the importance of quantum effects in γ-photon emission. Here, E_S is the Schwinger field given by

$$E_S = \frac{m_e^2 c^3}{e\hbar} \approx 1.32 \times 10^{18} \text{Vm}^{-1}. \tag{5}$$

The Schwinger field[5,6,19,27] is the field required to produce work of $m_e c^2$ over a distance of the Compton scattering wavelength, $\lambda_C = 2\pi\hbar/m_e c$. At this limit, virtual $e^- e^+$ pairs in vacuum can be separated, producing real $e^- e^+$ in a process known as Sauter–Schwinger[5,6,27] pair production. If $\chi_e \gg 1$, then the Compton scattering γ-photon emission is a multiphoton process,

$$e^{\pm} + N\omega_l \rightarrow e^{\pm} + \omega_\gamma. \tag{6}$$

The dimensionless Lorentz invariant parameter for γ-photon is χ_γ,

$$\chi_\gamma = \frac{\hbar\omega_l}{m_e c^2} \sqrt{\left(\frac{\boldsymbol{E}}{E_S} + \frac{c^2}{u_p}\hat{\boldsymbol{k}} \times \frac{\boldsymbol{B}}{E_S}\right)^2 - \left(\frac{c}{u_p}\hat{\boldsymbol{k}} \cdot \frac{\boldsymbol{E}}{E_S}\right)^2}, \tag{7}$$

where u_p is the phase velocity and $\hat{\boldsymbol{k}}$ is the wavevector unit vector. For larger χ_γ values, the probability of the multiphoton Breit–Wheeler $e^- e^+$ pair generation is increased.[28]

B. Intensity levels

A relativistic electron moving in the presence of an electromagnetic field results in γ-photon emission. The expression for radiation reaction force simplifies[19,28] if we assume that the emitting electron interacts with the antinodes of two colliding electromagnetic waves as the magnetic field cancels out. This assumption is also related to the interaction of a laser with a near-critical target by considering the reference frame that moves with the wave group velocity. This assumption allows us to find two intensity regimes.

In the non-linear Thomson scattering regime, the power emitted[29] by the electron is

$$P_\gamma = \varepsilon_{rad}\, m_e c^2 \omega_l \gamma_e^2 a_0^2 \gamma_e (\gamma_e^2 - 1)^{1/2} \approx \varepsilon_{rad}\, m_e c^2 \omega_l a_0^2 \gamma_e^2. \tag{8}$$

The maximum electron energy acquisition rate is

$$P_{acq} = m_e c^2 \omega_l a_0. \tag{9}$$

Radiation effects dominate[30] for

$$a_0 > a_{rad} = \varepsilon_{rad}^{-1/3}. \tag{10}$$

By requiring energy balance between Eqs. (8) and (9), then the condition $a_0 = a_{rad}$ corresponds to an intensity of

$$I_R = \left(\frac{3}{2}\right)^{2/3} \frac{m_e^{8/3} c^5 \omega_l^{4/3}}{2\pi (e/\sqrt{4\pi\varepsilon_0})^{10/3}} \approx 2.64 \times 10^{23} \left(\frac{1\,\mu\text{m}}{\lambda_l}\right)^{4/3} \text{W cm}^{-2}. \tag{11}$$

When the energy of the emitted γ-photon energy is comparable to the electron energy, then $\hbar\omega_\gamma \approx \gamma_e m_e c^2$ and QED effects become important. The energy of photons emitted by an electron circulating with frequency ω_l is $\hbar\omega_\gamma \approx \hbar\omega_l \gamma_e^3$.[19] Therefore, $\gamma_e = \sqrt{m_e c^2/(\hbar\omega_l)} \approx 642\sqrt{\lambda_l/(1\,\mu\text{m})}$. For laser intensities greater than 10^{23} Wcm^{-2}, the electron energy scales as $m_e c^2 (a_0/\varepsilon_{rad})^{1/4}$. As a result,[28,30] in the QED regime,

$$a_0 = \frac{2e^2/(4\pi\varepsilon_0) m_e c}{3\hbar\omega_l} = \left(\frac{2}{3}\alpha\right)^2 \varepsilon_{rad}^{-1}. \tag{12}$$

The corresponding electric field is

$$E_0 = \frac{2m_e^2 c^2 e/(4\pi\varepsilon_0)}{3\hbar^2} = \frac{2}{3}\alpha E_S, \tag{13}$$

where $\alpha = e^2/(4\pi\varepsilon_0\hbar c) \approx 1/137$ is the fine structure constant. This field, corresponds to a laser intensity of $\sim 1.1 \times 10^{25}$ Wcm^{-2}.

III. IMPLEMENTATION OF MONTE-CARLO METHOD FOR QED PIC CODES

γ-photon emission and $e^- e^+$ pair generation can be described by the Monte Carlo method,[31,32] thus capturing the statistical nature of these processes. While there are several ways to implement such a Monte Carlo algorithm, a computationally efficient method makes use of the cumulative probability of emission. The EPOCH QED module[33–35] is an example of this method. For a given particle, a random positive number less than or equal to unity is set to the cumulative probability at which emission will occur, $P(t) = 1 - \exp(-\tau_{em})$. Here, τ_{em} is the optical depth at which emission occurs and the previous equation is then inverted to yield the value of τ_{em} at which the particle will emit. For each particle the optical depth is updated according

to $\tau(t) = \int R(t)\,dt$, where $R(t)$ is the rate of the emission process. Emission occurs when $\tau = \tau_{em}$.

The required rates of γ-photon emission and e^-e^+ pair generation are given by assuming that the electric and magnetic fields are locally constant and crossed; for discussion on the validity of this approach see, e.g., Refs. 10 and 36–40. When backreaction on the background field is ignored the emitted photon momentum is balanced by the recoil of the emitting electron (or positron). When a γ-photon generates an e^-e^+ pair, its energy is shared between the electron and positron.

In a PIC code,[41–43] many real particles are represented by a single macroparticle in order that the computational cost of simulating the particles is not prohibitive. The momentum and position of each macroparticle is obtained by integration of the relativistic Lorentz equation. Subsequently, the charge and current values are obtained by interpolating the macroparticle positions and velocities onto a computational grid. These current and charge densities are then used to update the electric and magnetic field values in each cell via a discretization of Maxwell's equations. These updated fields are then used to update the momentum and position of the macroparticles in the next time step and so on in a computational loop.

The Monte Carlo approach to simulating γ-photon emission and e^-e^+ pair generation lends itself naturally to inclusion in a PIC code. In the resulting QED-PIC approach the electromagnetic fields are split into low (e.g., laser field) and high frequency (γ-ray) components.[35] The low frequency component is determined by solving Maxwell's equations in the usual way. The high frequency γ-ray component is discretized as macroparticles which propagate ballistically. The emission of these γ-ray macroparticles, by electrons and positrons (nonlinear inverse Compton scattering), as well as their subsequent generation of electron positron pairs (nonlinear Breit–Wheeler process), follows the Monte Carlo method outlined above.[33,44] More recently, this method has also been used to describe Bremsstrahlung[45–47] and Bethe–Heitler pair production.[46,48]

In addition to the Monte Carlo approach, a semi-classical model for γ-ray emission by nonlinear inverse Compton scattering has been included in some PIC codes.[35,44,49,50] Here, the electrons and positrons radiate continuously but the radiated intensity I is reduced by the Gaunt factor $G(\chi_e) = I/I_{cl}$ (where I_{cl} is the intensity radiated in a classical model).[35] A semiclassical model accurately captures the evolution of averaged quantities such as at the average energy loss, but it is less accurate than the Monte Carlo approach in describing quantities influenced by the stochasticity[35,51] of the QED processes. It can be useful, however, as a comparison to the Monte Carlo model to reveal the effects of quantum stochasticity, and in the development of theoretical models, where the inclusion of deterministic radiation is far more straightforward.[52,53]

IV. PARTICLE-IN-CELL γ-PHOTONS

During laser–matter interaction experiments at intensity levels of 10^{16} Wcm^{-2}, photon emission in the keV-range is reported[54] via the inverse Bremsstrahlung process, while by increasing the intensity to 10^{20} Wcm^{-2}, the MeV-range is obtained.[55] The following discussion is based on QED PIC simulations of femtosecond-class lasers focused to a micrometer scale focal spot interacting with matter, except where it is otherwise stated. The simulations are either one-dimensional or two-dimensional, except where 3D simulations are specified. These results, based on the interaction of ultra-intense lasers with ever more innovative targets, illustrate the continuously evolving effort to enhance the conversion efficiency of the laser energy into γ-photon energy, κ_γ.

A. Foil targets

A 10^{22} Wcm^{-2} intensity laser emits 0.2 % of its energy as high energy photons[56] when interacting with a 3 μm thick copper slab proceeded by an exponential preplasma. The preplasma gradient strongly affects the laser absorption efficiency. First, electrons are accelerated by the $\mathbf{E} \times \mathbf{B}$ force. The reflected laser field results in the second electron population. The third population is due to compensation of the $\mathbf{E} \times \mathbf{B}$ force by the longitudinal plasma field, where return currents (electrons) further increase the emitted radiation. When increasing the laser intensity by an order of magnitude, κ_γ increases to 20 %, fitted by $\kappa_\gamma \propto I^2$ for the intensities used.

A similar setup[57] uses an overcritical 10 μm thick foil with an added preplasma, interacting with a laser of $a_0 = 150$. The resulting γ-ray flash duration is comparable to that of the laser pulse. Existence of an optimal preplasma scale length is found, with a long preplasma being less prone to laser backreflection. A $\kappa_\gamma \approx 32\%$ is estimated, attributed to self-focusing of the laser which leads to enhancement of the field and consequent high laser depletion. Moreover, the emitted radiation occurs in two symmetric lobes.

When a 4×10^{23} Wcm^{-2} intensity laser interacts with a 1 μm thick aluminum foil,[33,34] the laser pressure bores a cavity into the foil, where both γ-photons and e^-e^+ pairs are created. A preplasma is found to enhance the γ-photon yield. The simulations result in $\kappa_\gamma \approx 10\,\%$ for a 12.5 PW laser and $\kappa_\gamma \approx 40\,\%$ for a 320 PW laser. Optimization of γ-photon yield relies on a preplasma multiparametric study,[58] where the variables include the laser power, pulse duration, focal spot, target thickness, and preplasma exponent factors. The optimal γ-flash generation occurs when the laser undergoes self-focusing in the preplasma. When the laser propagates within low density, the generated γ-photons are emitted backwards from electrons counter-propagating relative to the laser. This tendency reverses at denser preplasma regions. 3D simulations report $\kappa_\gamma \approx 20\,\%$ for the 10 PW case.

The importance of the proper electron density and foil thickness choice on optimizing γ-photon generation[59] is illustrated by the interaction of a 10^{22} Wcm^{-2} intensity laser with a foil having an electron density of either 1.87×10^{22} cm^{-3} (relativistically transparent, undercritical) or 1.1×10^{23} cm^{-3} (opaque, overcritical). For the undercritical target case, γ-photon production is associated with energetic electrons counter-propagating with the laser. The spatial distribution of the radiated power reveals periodic modulations attributed to relativistic Doppler effects, resulting in γ-ray bursts toward the target front. The γ-photon yield diminishes for foils thinner than 1 μm due to rapid target expansion. For overcritical targets, γ-photon generation occurs in regions defined by the expanding preplasma and/or the skin-depth layer. For a relatively thick foil, γ-photon emission occurs mainly at a broad angle with respect to the laser axis, in the forward direction, as a result of back-directed electrons to the target. For foils thinner than 1 μm, a maximal emission angle occurs at both the forward and backward directions, attributed to recirculating electrons.

For a comparable (to Ref. 59) simulation setup,[60] at a fixed density of 3.18×10^{23} cm^{-3}, but with various intensity values covering the range of $3 \times 10^{21} - 10^{23}$ Wcm^{-2}, the double-lobe pattern is

reaffirmed. The lobes are maximized at ∼30°, with the exact value depending on the target thickness.[60] For targets thicker than 2 μm, the γ-photon angular distribution saturates. A theoretical model[60] estimates the γ-photon emission angle by assuming that the incoming and reflected parts of the laser pulse form a planar standing wave. Within the intensity range examined, the γ-photon spectrum temperature increases linearly to the laser intensity.

The double-lobe γ-photon distribution is also observed[61] on simulations of a of 5.4×10^{23} Wcm^{-2} intensity laser interacting with a relativistically undercritical target. The laser penetrates the target forming a cavity. A periodic electron distribution is formed on the laser axis, dragging protons and forming quasineutral bunches. The radiation reaction force reaches values comparable to the ponderomotive force that classically expels electrons from the cavity region, and electrons are trapped in the laser field region. The sequential recoil of those trapped electrons results in γ-photons emitted at two directions ($15^\circ - 30^\circ$ and $330^\circ - 345^\circ$), with $\kappa_\gamma \approx 35$ %.

The γ-photon emission angle has also been investigated through the transition[62,63] from the Light-Sail (thin targets) to the Hole-Boring (thick targets) regime, where a 2×10^{23} Wcm^{-2} intensity laser interacts with an aluminum target, varying in thickness from 50 to 400 nm. The Hole-Boring regime allows strong electron return currents resulting in γ-photon emission. Due to strong charge separation fields, the longitudinal electron momentum acquires large values, decreasing the γ-photon emission angle.

B. Structured targets

In the relativistically transparent regime, at non-optimal plasma densities, the laser deviates from its propagation axis and the emitted γ-photons are non-directional. To overcome this issue,[64] an undercritical channel is added to an overcritical target that interacts with a 5×10^{22} Wcm^{-2} intensity laser. A slowly varying magnetic field appears within the channel. Due to self-generation of the magnetic field, electrons moving within the channel feel an enhanced accelerating force, increasing the γ-photon yield. The laser–target interaction under this scheme demonstrates $\kappa_\gamma \approx 15$ %. The emission occurs near the channel walls, at the electron trajectory turning points. Therefore, γ-photon emission occurs at γ-ray bursts of period same as that of the laser. 3D simulations verified the two-lobed γ-photon emission pattern, although κ_γ dropped to 3.5 %.

In the channel targets, by increasing the laser power the deviation of the lobes from the laser axis decreases.[65] For a 4 PW laser $\kappa_\gamma \approx 1.5$ %. The number of γ-photons is proportional to P^2 for $P < 4$ PW, and proportional to P for $P > 4$ PW. A model finding optimal conditions for γ-photon emission by channel targets has been constructed,[66] where the number of γ-photons scales proportionally to the laser energy, and $\kappa_\gamma \propto a_0^3$. If the cylindrical target is combined with Poincaré beams,[67] emission of collimated γ-photons is expected.

In a diametrically opposite target design,[68] irradiation of a 3D long thin wire by a 2.5×10^{22} Wcm^{-2} intensity laser is proposed for efficient γ-photon generation. The findings suggest $\kappa_\gamma \approx 10\%$. The rectangular aluminum wire has an 0.6 μm edge. The laser–wire interaction initiated before the laser reached the focal spot, to gradually accelerate electrons along the wire direction with their divergence reduced, resulting in the existence of a collimated electron population at the time when the pulse reaches its highest intensity on the focal spot. The resulting γ-photons are highly collimated, with a maximum energy of 500 MeV.

A hybrid scheme[69] for γ-photon emission, as a first stage, employs a channel filled with a low plasma density. The density has a transversely paraboloidal profile and so propagation of the laser in the channel results in a collimated high energy, high density electron beam. The second stage employs a higher density plasma region, attached to the low density plasma channel. In the vicinity of the electron beam, strong electrostatic fields are formed, corresponding to $\chi_e \approx 0.1$. The high χ_e value of the directional electron beam results in a collimated γ-photon beam, where for a 10 PW laser a $\kappa_\gamma \approx 16\%$ is reported.

A 3D scheme based on reflection of a circularly polarized laser[70] of 1.4×10^{22} Wcm^{-2} intensity employs a cylindrical micro-channel target attached to a square foil consisting of eight triangular segments (height difference of $0.25\pi\lambda_l$) joined in the center of the square. The triangular segments result in a phase difference of the reflected pulse and transformation of the beam to a Laguerre–Gaussian beam. Prior to reflection, electrons are dragged out from the micro-channel walls and accelerated by the longitudinal field formed in the channel, where the micro-channel acts as an optical waveguide. Interaction of the accelerated electrons with the reflected (to the square foil) pulse results in a collimated γ-photon beam with a $\kappa_\gamma \approx 1.2\%$.

Micro-fabrication of a conical structure attached to a foil target is proposed,[71] interacting with a 2×10^{22} Wcm^{-2} laser. The γ-photon production from both Bremsstrahlung and Compton scattering is considered, where their contribution is compared by employing both aluminum and gold targets. For gold targets Bremsstrahlung produces more γ-photons than Compton scattering. On the other hand, Compton scattering contribution dominates for aluminum targets. The cone target benefits γ-photon emission due to the magnetic and electrostatic fields generated within the cone, resulting in enhanced hot electron channeling.

The double-layer target concept is examined for γ-photon emission,[72] during the target interaction with a 3×10^{23} Wcm^{-2} intensity laser. The front target layer consists of a 22 μm thick hydrogen plasma of 4.5×10^{21} cm^{-3} electron density, followed by a 1 μm thick gold foil. While the laser propagates into the hydrogen region it traps electrons, accelerating them to relativistic energies along the laser axis. Part of the laser is reflected by the gold foil and Doppler-shifted, forming attosecond pulses. Furthermore, deformation of the gold surface acts as a concave mirror. The reflected field, when interacting with the hot electrons propagating toward the laser axis, results in collimated γ-photon emission. For the 3D simulation case, $\kappa_\gamma \approx 1.4$ % is obtained.

A structured target[73] for enhancing κ_γ consists of four symmetric carbon microwires attached on an aluminum foil, acting as a reflector to the laser pulse. In that study, optimal 3D PIC simulations use microwires of 12 μm length, 1 μm diameter, and 3.5 μm spacing. The simulations employ a 50 PW laser, at an intensity of 8×10^{23} Wcm^{-2}. As the laser propagates between the wires it expels electrons, that are then accelerated along the laser propagation direction at cutoff energies of 1.5 GeV. By that time, γ-photon emission is low, attributed to the transversely oscillating electron motion. When the laser pulse is reflected by the aluminum foil, $\kappa_\gamma \approx 27$ % is rapidly reached. The simulations reaffirm the appearance of the typical double-lobe structure of the emitted γ-photons.

A flat foil irradiated by a low amplitude field (several orders of magnitude lower than the main laser pulse) is proposed for enhancing

γ-photon emission.[75] The foil irradiation can be attributed either to the laser amplified spontaneous emission or to a secondary low power laser. Magneto-hydrodynamic simulations demonstrate that if for a specific target material the appropriate secondary field is chosen, then a controllable conical-like cavity is tailored on the target.[74] In addition to cavitation of the target, an exponential-like preplasma distribution is formed on the target front region. The resulting density distributions, as shown in Fig. 1, are used as initial conditions in 3D PIC simulations. The simulations are performed at several power levels, at the range of $1 - 10$ PW. The proposed scheme benefits from the combination of isolated aspects previously studied, as near-critical density targets,[64] conical targets,[71] and preplasma effects.[58]

The tailored conical-like cavity is of diameter comparable to the focal spot diameter. As a result, most of the laser field is confined within the cavity, increasing its intensity by an order of magnitude. Although for a 10 PW laser, an intensity of 2.8×10^{23} Wcm^{-2} is expected on focus, intensities of 2.6×10^{24} Wcm^{-2} are recorded in the simulations, reaching the regime of prolific γ-photon generation by already existing lasers. Moreover, reflection of the incident laser by the cavity walls results in the appearance of a strong longitudinal electric field component, that assists further cavitation of the foil, as seen in Fig. 2, allowing existence of ultraintense fields for an extended time. The extreme intensities reached fall in the relativistically transparent regime for lithium. As a result, the laser field penetrates deep into the target, depleting almost all of its energy. For the 10 PW case, a $\kappa_\gamma \approx 30\,\%$ is reported for a lithium tailored target, decreasing to $\kappa_\gamma \approx 19\,\%$ for a flat foil target. This is reflected on the γ-photon energy

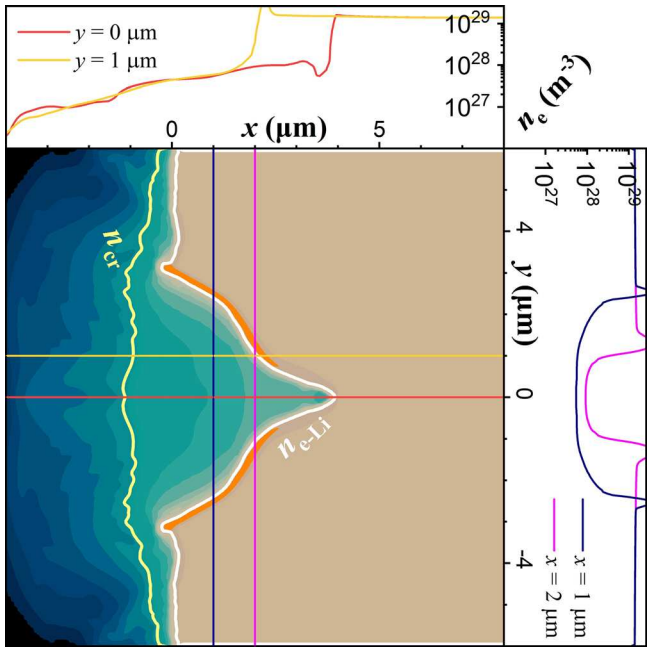

FIG. 1. Electron number density obtained by magneto-hydrodynamic simulations[74] following irradiation of a lithium foil, used as initial conditions for PIC simulations.[75] The yellow contour line is at the critical density and the white contour line is at the lithium solid electron density. The orange saturated contour is overcritical for laser intensities above 10^{23} Wcm^{-2}. Reproduced with permission from Hadjisolomou *et al.*, Sci. Rep. **12**, 17143 (2022).[75] Copyright 2022 Springer Nature Group.

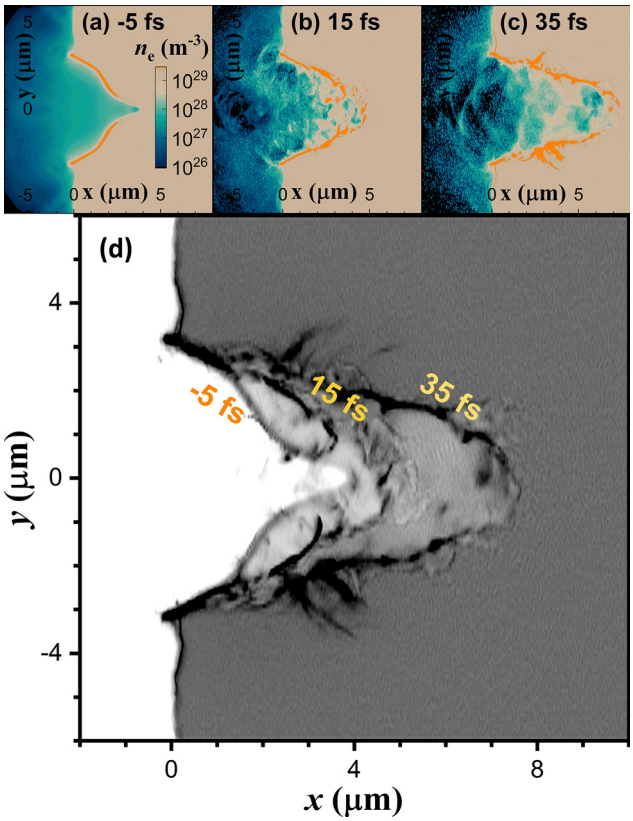

FIG. 2. Electron number density at (a) −5, (b) 15, and (c) 35 fs, where the orange region is overcritical for field intensity below 10^{23} Wcm^{-2}. (d) Overlay of three successive electron number density distributions, with a time step of 20 fs. The first layer is at −5 fs, when the main pulse is within the cavity. Reproduced with permission from Hadjisolomou *et al.*, Sci. Rep. **12**, 17143 (2022).[75] Copyright 2022 Springer Nature Group.

spectra, as shown in Fig. 3. The figure compares the cases for tailored targets (solid lines) vs foil targets (dashed lines) for laser powers of 1, 5, and 10 PW. In all power levels examined, the tailored targets result in significantly enhanced γ-photon energy spectra compared to the foil targets. For the 10 PW case, usage of tailored targets increased the γ-photon temperature from 45 MeV (for foil) to 60 MeV. In both cases, the emitted γ-photons are in the GeV-level. Moreover, if a material denser than lithium is used then κ_γ decreases since the laser–target interaction moves out of the relativistically transparent regime.

The double-lobe γ-photon emission pattern is verified, with emphasis given on both the spatial and temporal structure of the γ-flash. The γ-photon emission angle is found to be maximized at angles within the range $37° - 55°$. At all laser power levels the tailored targets (compared to foil targets) give optimal emission angles closer to the laser axis, while the emission angle decreases for increasing laser power. Temporal analysis of the γ-flash reveals a direct connection of γ-photon emission with the peaks of the laser field, as shown in Fig. 4. Two symmetric emission patterns (with respect to the laser axis) are observed at the two laser polarization hemi-planes, shifted by half wavelength and being suppressed along the laser axis. This pattern is explained by γ-photon emission by electrons co-moving (at a certain

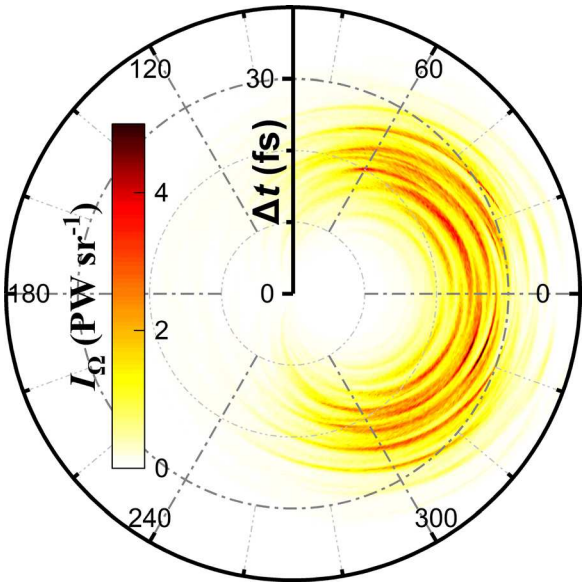

FIG. 3. Radiant intensity of γ-photons with respect to the polarization plane, as a function of time-of-flight difference. Reproduced with permission from Hadjisolomou *et al.*, Sci. Rep. **12**, 17143 (2022).[75] Copyright 2022 Springer Nature Group.

angle) with the laser pulse. When the electron momentum angle approaches zero then γ-photon emission is suppressed, forming the double-lobe structure.

C. Multiple laser beams schemes

For the case of a plane electromagnetic wave, the parameter χ_e that controls the γ-photon emission (see Sec. II A) is maximized for a

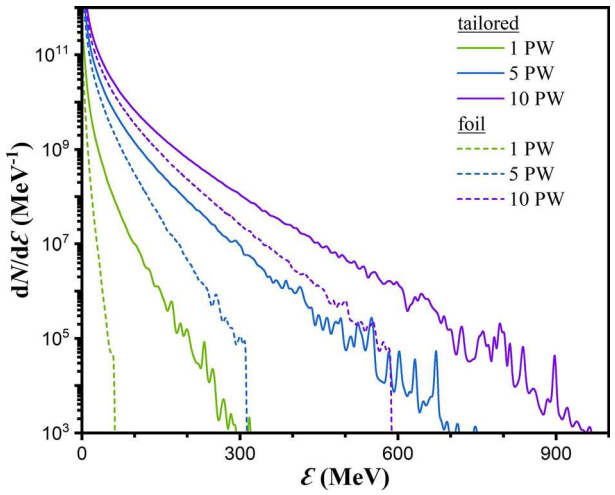

FIG. 4. γ-photon energy spectra resulting from the interaction of PW-class (power noted on the figure legend) laser with a lithium target. The cases of tailored targets (solid lines) are compared with those for foil targets (dashed lines). Reproduced with permission from Hadjisolomou *et al.*, Sci. Rep. **12**, 17143 (2022).[75] Copyright 2022 Springer Nature Group.

charged particle if its momentum is antiparallel to the wave propagation direction, and zero if it is parallel. This observation naturally brought into the discussion the use of multiple colliding lasers to achieve higher χ_e compared to single beam schemes where in the latter case electrons and positrons are often primarily accelerated in the direction of propagation of the laser.

The interaction of two antiparallel 12.5 PW power, 4×10^{23} cm^{-2} intensity lasers with an aluminum foil is proposed.[76] The dual-beam foil irradiation results in symmetric target compression, reducing the number of hot electrons escaping the target. The dual-beam case corresponds to $\kappa_\gamma = 20.2\,\%$, an increase in a factor of three compared to the corresponding single-beam case. Overlapping of the incident and reflected pulses results in standing waves, altering χ_e. Moreover, symmetric compression shapes the foil to a concave mirror, allowing higher reflected laser intensities. In addition, electrons from either side of the foil crossover to the opposite side, counter-propagating to the opposite laser. The aforementioned factors enhance γ-photon emission. A similar setup proposes an orthogonal set of polarisations.[52] The target consists of a 1 μm thick, relativistically over-critical foil. When QED effects are ignored, the two pulses eventually bore through the foil. When QED effects are included, however, the two pulses do not bore through the foil. This is attributed to enhanced laser absorption resulting from radiation reaction.

3D simulations of two antiparallel linearly polarized lasers interacting with a liquid hydrogen slab are compared at the levels of $a_0 = 1000$ and $a_0 = 2000$.[77] This setup results in an enhancement of γ-photon emission, which is attributed to formation of standing waves by the overlapping lasers. For $a_0 = 1000$ the γ-photons are emitted mainly at $\pm 90°$, while for $a_0 = 2000$, they are emitted at $\pm 30°$ and $\pm 150°$.

Combination of the 3D dual-beam scheme with structured targets is also considered.[78] Each 3×10^{22} Wcm^{-2} intensity laser is incident on a conical target filled with near critical plasma. The use of this target geometry exhibits a laser intensification of approximately ten times. The laser propagating in the near critical plasma enters the radiation trapping regime.[61] As the damping force equals the Lorentz force then electrons pileup on the laser axis. The result of electron bunching is the induction of a poloidal self-generated magnetic field that keeps electrons on axis. This electron population propagates along with the laser pulse in an oscillatory motion emitting γ-photons. When the two pulses collide with the opposite electron population, further γ-photon emission occurs.

Collision of two counter-propagating circularly polarized pulses of same spatial profile but different temporal profile, propagating in a near-critical plasma, is also investigated.[79] The 3D scheme reports $\kappa_\gamma \approx 8\%$ at an intensity of 2×10^{22} Wcm^{-2}.

The dual-beam scheme is extended in a quadruple-beam scheme.[80] The optimal polarization configuration (of the linearly polarized lasers) for γ-photon emission corresponds to the counter-propagating laser pulses being of the same polarization but polarized orthogonally to the other two laser pulses. Each laser has a spot size significantly larger than the 0.3 μm wide target used. The parameter a_0 ranges from 500 to 2000. For $a_0 > 800$ the γ-photon emission growth rate is lower than predicted,[77] indicating disruption of the standing waves.[81,82] For 10^{24} cm^{-2} intensity, $\kappa_\gamma \approx 50\,\%$, which is attributed to the high γ-photon emission growth rate of the configuration. Most of the γ-photon energy is radiated in a cross-like pattern. This laser configuration has been also considered for an order of magnitude lower

intensities and a significantly larger target,[83] where for a $a_0 = 325$ laser a $\kappa_\gamma \approx 53.7\%$ is reported.

Interaction of two 3D elliptically polarized lasers with two 0.32 μm thick diamond-like foils is proposed.[84] Although circularly polarized beams benefit the radiation pressure acceleration mechanism, elliptically polarized lasers reduce the transverse instabilities. The two ellipse axis correspond to a_0 values of 237 and 154. The laser–foil interaction forms a conical-like structure in the foil before the pulse peak amplitude interacts with the target. During that stage, an electron population is dragged from the cavity walls and then interacting with the reflected waves, but with a low γ-photon yield due to Doppler shifting of the reflected laser. Following the foil cavitation, the target deforms, lowering its density along the laser axis. If the spacing of the foils is suitably chosen, the time the two pulses penetrate the foils coincides with the time the two foil front surfaces collide. Hot electrons crossover to the opposite pulse region, resulting in high χ_e values, enhancing γ-photon emission by a factor of four compared to the single-foil interaction under the same conditions.

An alternative to double-foils is the convex target,[85] interacting with a 4×10^{23} cm^{-2} intensity laser. The targets consist of 2 μm thick aluminum. The two foils have a separation distance of 2 μm, the same as that of the convex targets in the center. The results indicate an 11% γ-photon emission enhancement for the convex targets case, reaching $\kappa_\gamma \approx 13.2\%$.

Counter-propagating laser beams can pose a risk of optical damage to the opposed laser beam. However, this issue can be suppressed by using a series of Faraday isolators. Alternatively, a setup of three beams (or any geometry where two laser beams do not lie on the same propagation axis) can be used.

D. The λ^3 scheme—An alternative to multi-beam configurations

The usage of multi-beam configurations significantly enhances γ-photon emission from the interaction of intense lasers with matter. The 4π-spherical focusing scheme can be regarded as an extreme case of either multiple laser beam focusing or tight focusing scheme.[87] Focusing a large number of single-cycle pulses to a single spot mimics the λ^3 regime,[88] that provides the highest possible laser intensity for the least energy, at a given power. The utility of the λ^3 regime for studying QED effects during the interaction of an ultraintense laser with a target has recently been demonstrated[86,89] in a 3D multiparametric study, where a sample case of the λ^3 laser fields used are shown in Fig. 5. The varying parameters include the laser polarization, target thickness, target electron density and laser power.

The simulations suggest substantial enhancement in the emission of γ-photons, compared to multi-beam (≥ 4) schemes. At a laser intensity of 10^{25} cm^{-2}, corresponding to $a_0 \approx 2700$ and reached by an 80 PW laser, optimal conditions for γ-photon emission occur for a radially polarized laser combined with a 2 μm thick titanium target. Under these conditions, a $\kappa_\gamma \approx 47\,\%$ is recorded, as shown in Fig. 6. After parameter optimization, a linearly polarized laser gives $\kappa_\gamma \approx 42\,\%$ and an azimuthally polarized laser (magnetic field rotates around the laser propagation axis) gives $\kappa_\gamma \approx 29\,\%$.

The high κ_γ for radially polarized lasers is attributed to the dominant longitudinal field component that increases the laser coupling to the target.[90] Although the intensity of a linearly polarized laser when tightly focused is double that of a radially polarized laser, the former has a smaller longitudinal electric field component.[91] By definition, for the azimuthally polarized laser no longitudinal electric field exists. This field component drives the formation of a cavity in the foil. The cavity is symmetric and has a conical-like form for the radially polarized laser case. The case of linearly polarized laser corresponds to a square-like cavity. The cavity formation is significantly delayed for the azimuthally polarized laser case. In the case of the radially polarized laser case, reflection, diffraction, and interference of the laser field in the cavity results in a peak intensity of 8.8×10^{25} Wcm^{-2}.

For the radially polarized laser case, several distinct energetic electron populations are identified. These groups are directed at 0°, 180°, and 60° and are characterized by the quarter-period.

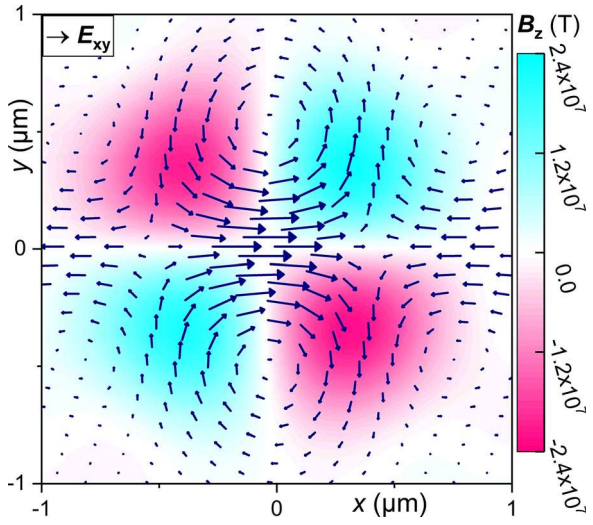

FIG. 5. The λ^3 radially polarized laser fields. The black arrows correspond to the electric field vectors, over-plotted on a contour of the magnetic field. Reproduced with permission from Hadjisolomou *et al.*, J. Plasma Phys., **88**, 905880104 (2022).[86] Copyright 2022 Cambridge University Press.

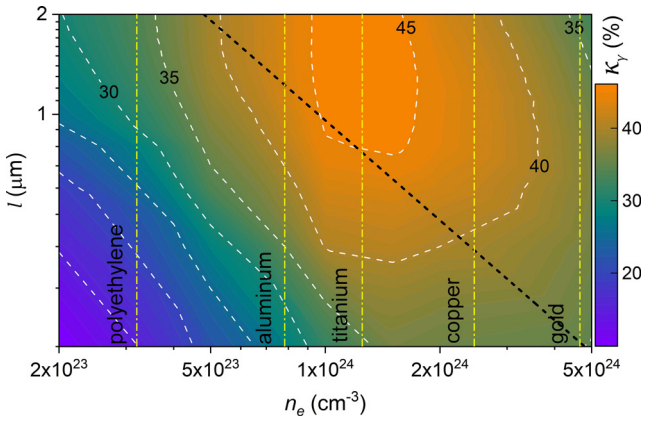

FIG. 6. κ_γ as a function of the target thickness and electron density.[89] The black dashed line follows the relation between target thickness and electron density for optimal laser coupling to the target.[90] Reproduced with permission from Hadjisolomou *et al.*, Phys. Rev. E **104**, 015203 (2021).[89] Copyright 2021 American Physical Society.

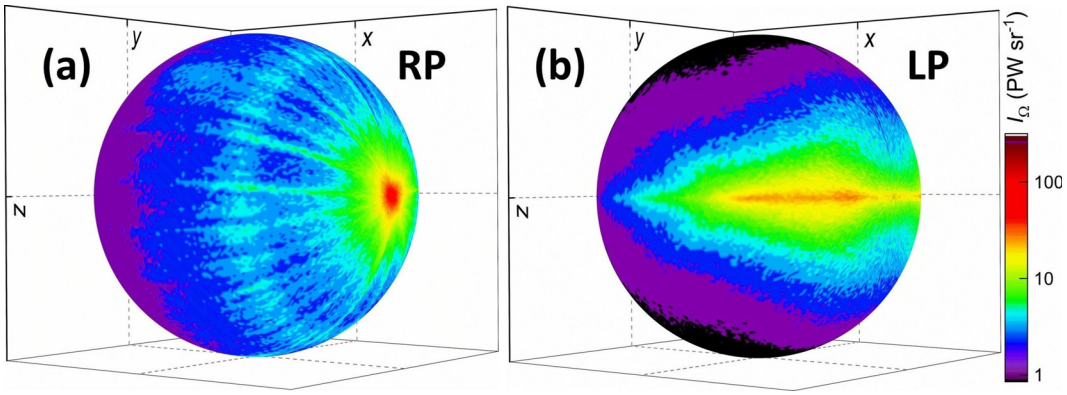

FIG. 7. γ-photon radiant intensity for (a) a RP laser and (b) a LP laser. Reproduced with permission from Hadjisolomou *et al.*, J. Plasma Phys. **88**, 905880104 (2022).[86] Copyright 2022 Cambridge University Press.

The emission of high energy γ-photons is identified along the same directions, during the same time instances. The radially polarized laser case exhibits an extremely collimated γ-photon population along the laser axis, a secondary population on the opposite direction and a third but minor population at 60°, as seen in Fig. 7. For the linearly polarized laser case, a double-lobe structure is observed. For the azimuthally polarized laser case, the γ-photon emission is more isotropic.

The γ-photons propagate ballistically within an expanding spherical shell. By calculating the γ-photon standard deviation, it is estimated that the radially, linearly and azimuthally polarized lasers correspond to γ-flashes of 31, 28, and 13 PW, respectively. Variation on the laser power reveals that κ_γ follows a saturating function. By decreasing the target density, the threshold for observing γ-photon emission shifts to lower power values.

Various schemes for enhancing γ-photon yield presented in Sec. IV are summarized in Table I and Fig. 8.

V. RADIOACTIVE NUCLEI AND ELECTRON–POSITRON PAIR PRODUCTION BY IRRADIATING HIGH-Z TARGET WITH γ-PHOTONS

FLUKA[92,93] Monte Carlo simulations are suitable to examine the effect of γ-photons, electrons, positrons and ions interacting with a High-Z target.[17] The Monte Carlo simulations import as primary particles the PIC output (position, momentum, and weight) macroparticles [γ-photons, electrons, positrons, titanium ions (Ti^+)] corresponding to the optimal κ_γ case[89] described in Sec. IV D. The number of primary γ-photons approximately equals that of electrons, with Ti^+ and positrons being one and two orders of magnitude less, respectively. All PIC macroparticles apart from positrons are collimated along the laser axis due to the radially polarized laser used.

A 100 mm diameter lead ($^{207.19}$Pb) cylindrical target is placed 1 mm away from the focal spot. Lead, due to its high Z-number, benefits from high cross-section for e^-e^+ pair generation and for the giant dipole resonance (GDR). The target thickness varies from 1 to 100 mm. The energy deposited by the primary particles saturates for a 100 mm thick target.

When γ-photons collide with the target the ratio of the number of the emitted electrons to positrons is approximately unity, attributed to e^-e^+ pair generation. Positron generation is optimal for a 5 mm thick target, with the number of available positrons increased by a factor of 16 compared to the primary positrons. Target irradiation by the directional primary particles is reflected in the generation of collimated positrons.

Neutrons are produced via photonuclear reactions. The interactions are either direct (by initial γ-photons) or indirect (by Bremsstrahlung secondary γ-photons). For lead, photonuclear interactions cross-section peaks at 13 MeV. High neutron fluxes are required for neutron diffraction,[94] neutron resonance spectroscopy[95,96] and nuclear waste management.[97]

In the 100 mm thick target, residual nuclides are produced via photonuclear reactions, as seen in Fig. 9. The produced ^{203}Pb decays via electron capture to ^{203}Tl, with a half-life of 52 h. Since no hadron is involved in the decay, ^{203}Pb suits medical imaging.[98] Similarly, the produced ^{201}Tl decays via electron capture to ^{201}Hg, also suitable for medical imaging.[99]

VI. ALL-OPTICAL NONLINEAR BREIT–WHEELER PAIR PRODUCTION

An important future application of high-energy γ-photons generated with multi-PW laser systems is the study of photon–photon interactions in quantum electrodynamics (see the recent review Fedotov *et al.*[100]). In particular, nonlinear Breit–Wheeler pair production[7,11–13] requires large numbers of high-energy γ-photons to overcome the pair creation energy threshold and provide a sufficient signal to enable experimental observation.

The increase in both the conversion efficiency and maximum photon energy of the γ-ray flash with structured targets was recently exploited[101] to provide a simple all-optical setup for experimentally studying nonlinear Breit–Wheeler pair production at current and next generation high-power laser facilities. The proposed setup consisted of two stages, shown schematically in Fig. 10(a). First, a lithium target is irradiated with a combination of a nanosecond-duration prepulse and a high-intensity main laser pulse. The nanosecond-duration prepulse generates a conical channel in the lithium target which leads to an intensity enhancement of the main pulse, subsequently resulting in increase in the total yield and energy of γ-photons produced, as described above in Sec. IV B. Second, the

TABLE I. Comparison of the several schemes described in this work, proposed for enhanced yield of γ-photon emission.

Reference	Dimensions	Setup	Number of laser pulses	Power (PW)	κ_γ (%)
Nakamura *et al.*[57]	2D	Preplasma and foil target	1	1–10	3–32
Ridgers *et al.*[34]	2D	Preplasma and foil target	1	1.3–30	10–40
Lezhnin *et al.*[58]	2D	Preplasma and foil target	1	1–40	10.2–38
Lezhnin *et al.*[58]	3D	Preplasma and foil target	1	10	20
Vyskocil *et al.*[60]	2D	Preplasma and foil target	1	0.8–8	0.05–5.3
Ji *et al.*[61]	3D	Undercritical target	1	0.8–150	0.1–27
Luo *et al.*[76]	2D	Foil target	1	12	7
Stark *et al.*[64]	2D	Channeled target	1	5	15
Stark *et al.*[64]	3D	Channeled target	1	5	3.5
Wang *et al.*[65]	3D	Channeled target	1	1–10	1.2–3.8
Younis *et al.*[67]	3D	Channeled target	1	4	14
Wang *et al.*[68]	3D	Wire target	1	0.5–5	1.7–13
Zhu *et al.*[69]	3D	Preplasma plus foil target	1	1–6	2.7–16
Zhang *et al.*[70]	3D	Channeled target plus structured foil target	1	0.4–3	0.03–2.6
Gu *et al.*[72]	3D	Preplasma and foil target	1	25	1.5
Zhang *et al.*[73]	3D	Wire array plus foil target	1	20–60	12–40
Hadjisolomou *et al.*[75]	3D	Preplasma and foil	1	1–10	4.3–30
Luo *et al.*[76]	2D	Colliding pulses and foil target	2	25	20
Zhu *et al.*[78]	3D	Colliding pulses and conical target	2	3–150	6.4–37
Zhu *et al.*[79]	3D	Colliding pulses and nearcritical target	2	4.5–40	1.4–7
Vranic *et al.*[80]	2D	Colliding pulses and cluster target	4	20–350	3–76
Gong *et al.*[83]	2D	Colliding pulses and circular target	4	1.5–15	16–54
Li *et al.*[84]	3D	Colliding pulses and foil target	2	50	5.5
Yasen *et al.*[85]	2D	Convex target	2	3	13
Hadjisolomou *et al.*[86]	3D	λ^3-scheme	1	1–300	2.8–55

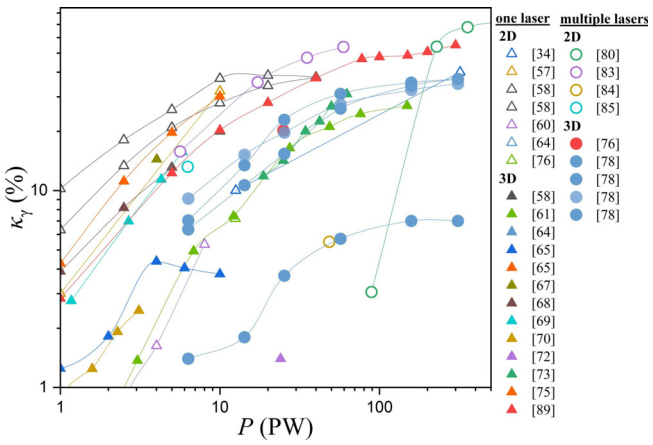

FIG. 8. κ_γ as a function of laser power, with data extracted from the references cited in this paper as shown in the figure legend. The correspondence for hollow triangles is for 2D single laser simulations, solid triangles is for 3D single laser simulations, hollow circles is for 2D multiple lasers simulations and solid circles is for 3D multiple lasers simulations.

produced γ-photons collide with a secondary counter-propagating high-intensity laser pulse to produce e^-e^+ pairs via the nonlinear Breit–Wheeler process.

Synchronization between the two stages can be achieved by splitting the total available laser pulse energy E_{total} into two beams, one to drive the γ-photon production with pulse energy E_{flash} and one to generate e^-e^+ pairs via the nonlinear Breit–Wheeler process with pulse energy E_{pairs}. Three different cases for the total available laser energy were considered, $E_{\text{total}} = (170, 510, 1700)$ J, which for a pulse duration of 17 fs corresponds to a power of $(10, 30, 100)$ PW, respectively.

Figure 10(b) shows the total number of e^-e^+ pairs expected per shot for each E_{total} as a function of the distance, d, from the photon point source at the lithium target rear surface to the focus of the secondary laser pulse. In each case, the ratio $\Delta = E_{\text{flash}}/E_{\text{pairs}}$, gives the relative splitting of the total available pulse energy into the two stages of the setup, where the optimal number of e^-e^+ pairs occurs for the case $\Delta = 1$. The total number of e^-e^+ pairs with a propagation distance $d = 10$ cm was shown to offer comparable numbers of pairs per shot to alternative schemes based on Bremsstrahlung photon generation (see, e.g., Ref. 102).

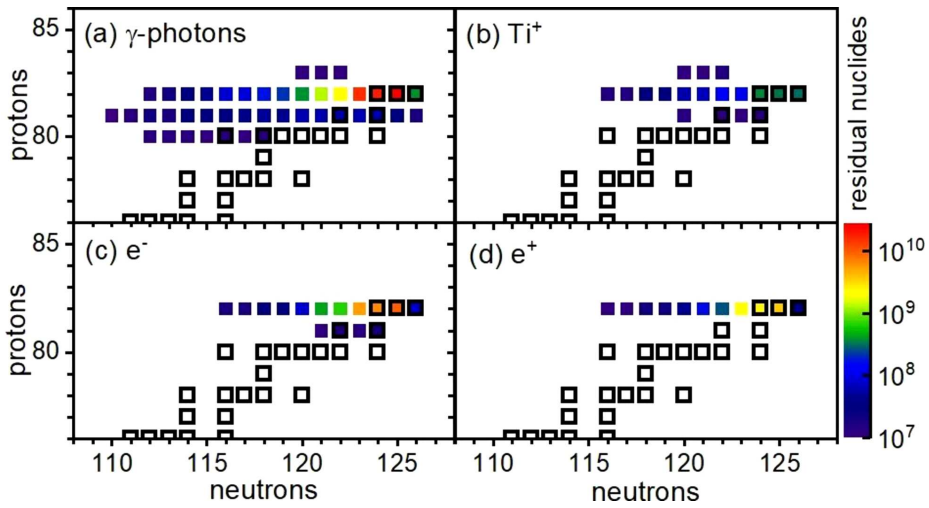

FIG. 9. Chart of residual nuclides obtained from MC simulation per λ^3-pulse.[17,86] Independent contribution from primary γ-photons, Ti^+, electrons and positrons is presented in (a)–(d), respectively. Stable nuclides are highlighted with a black frame. Reproduced with permission from Hadjisolomou *et al.*, J. Plasma Phys. **88**, 905880104 (2022).[86] Copyright 2022 Cambridge University Press.

VII. SUMMARY AND CONCLUSIONS

The discussion of QED effects in laser–matter interactions occupies a large volume of the laser plasma physics literature.[19,26,31,100,103–105] The proportion of the literature devoted on computational description of those effects increases alongside available computational power. In this article, we present recent results of the QED PIC literature.

We distinguish interactions of ultra-intense lasers with targets, both in the context of targets with preplasma and structured targets, both exhibiting a prolific γ-photon emission. Often, the suggested targets increase γ-photon emission by increasing the laser intensity, as for example by near-critical, conical, or tailored targets.

Emission of γ-photons is suppressed if the emitting electron moves in the same direction as the laser. As a result, multi-beam setups are suggested, demonstrating significant enhancement of γ-photon emission. An alternative to the multi-beam setup is the tight focusing scheme. This scheme, generalized in the λ^3 regime, demonstrates κ_γ values only comparable to that of four-beam (or higher) configurations.

The results of the λ^3 QED PIC simulations combined with Monte Carlo simulations illustrate a drastic effect of the primary laser–target interaction on high-Z materials, with significant increase in the generated positron number by the Bethe–Heitler process and strong activation of the high-Z material mainly due to photonuclear reactions. Moreover, one can harness the γ-ray flash properties to demonstrate the Breit–Wheeler pair production process based in an all-optical setup.

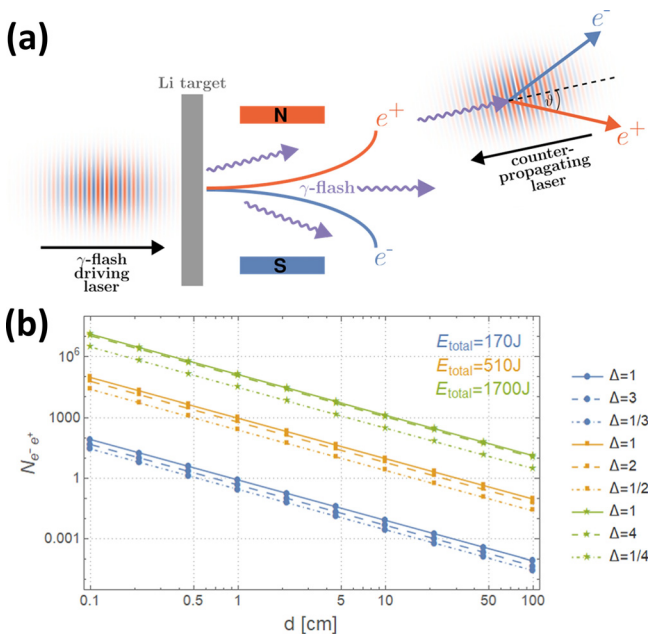

FIG. 10. (a) The proposed all-optical nonlinear Breit–Wheeler pair production setup. (b) The total number of e^-e^+ pairs expected per shot for each E_{total} as a function of the distance, d, from the photon point source at the lithium target rear surface to the focus of the secondary laser pulse. Reproduced with permission from MacLeod *et al.*, Phys. Rev. A **107**, 012215 (2023).[101] Copyright 2023 American Physical Society.

ACKNOWLEDGMENTS

The authors would like to acknowledge useful communication with A. S. Pirozhkov, T. Z. Esirkepov, M. Kando, and T. Kawachi. This work is supported by the project "Advanced research using high intensity laser produced photons and particles" (ADONIS) \allowbreak{(CZ.02.1.01/\allowbreak0.0/0.0/16 019/0000789)} from the European Regional Development Fund. C. P. Ridgers would like to acknowledge support from the UK Engineering and Physical Sciences Research Council, Grant No. EP/V049461/1.

AUTHOR DECLARATIONS

Conflict of Interest

The authors have no conflicts to disclose.

Author Contributions

Prokopis Hadjisolomou: Conceptualization (equal); Writing – original draft (lead); Writing – review & editing (equal). **Tae Moon Jeong:** Conceptualization (equal); Writing – review & editing (equal).

David Kolenatý: Writing – original draft (equal); Writing – review & editing (equal). **Alexander Macleod:** Writing – original draft (equal); Writing – review & editing (equal). **Veronika Olšovcová:** Writing – review & editing (equal). **Roberto Versaci:** Writing – review & editing (equal). **Christopher Ridgers:** Conceptualization (equal); Writing – original draft (equal); Writing – review & editing (equal). **Sergei V. Bulanov:** Conceptualization (lead); Writing – review & editing (equal).

DATA AVAILABILITY

Data sharing is not applicable to this article as no new data were created or analyzed in this study.

REFERENCES

[1]C. Radier, O. Chalus, M. Charbonneau, S. Thambirajah, G. Deschamps, S. David, J. Barbe, E. Etter, G. Matras, S. Ricaud *et al.*, "10 PW peak power femtosecond laser pulses at ELI-NP," High Power Laser Sci. Eng. **10**, e21 (2022).

[2]J. W. Yoon, Y. G. Kim, I. W. Choi, J. H. Sung, H. W. Lee, S. K. Lee, and C. H. Nam, "Realization of laser intensity over 10^{23} W/cm^2," Optica **8**, 630–635 (2021).

[3]D. Papadopoulos, J. Zou, C. L. Blanc, G. Chériaux, P. Georges, F. Druon, G. Mennerat, P. Ramirez, L. Martin, A. Fréneaux *et al.*, "The Apollon 10 PW laser: Experimental and theoretical investigation of the temporal characteristics," High Power Laser Sci. Eng. **4**, e34 (2016).

[4]C. N. Danson, C. Haefner, J. Bromage, T. Butcher, J. F. Chanteloup, E. A. Chowdhury, A. Galvanauskas, L. A. Gizzi, J. Hein, and D. I. Hillier, "Petawatt and exawatt class lasers worldwide," High Power Laser Sci. **7**, e54 (2019).

[5]F. Sauter, "Uber das Verhalten eines Elektrons im homogenen elektrischen Feld nach der relativistischen Theorie Diracs," Z. Phys. **69**, 742–764 (1931).

[6]W. Heisenberg and H. Euler, "Consequences of Dirac's theory of positrons," Z. Phys. **98**, 714–732 (1936).

[7]A. I. Nikishov and V. I. Ritus, "Quantum processes in the field of a plane electromagnetic wave and in a constant field. Part I," Sov. Phys. JETP **19**, 529–541 (1964), available at http://jetp.ras.ru/cgi-bin/dn/e_019_02_0529.pdf.

[8]L. S. Brown and T. W. B. Kibble, "Interaction of intense laser beams with electrons," Phys. Rev. **133**, A705–A719 (1964).

[9]I. I. Goldman, "Intensity effects in Compton scattering," Phys. Lett. **8**, 103–106 (1964).

[10]V. I. Ritus, "Quantum effects of the interaction of elementary particles with an intense electromagnetic field," J. Sov. Laser Res. **6**, 497–617 (1985).

[11]G. Breit and J. A. Wheeler, "Collision of two light quanta," Phys. Rev. **46**, 1087–1091 (1934).

[12]H. R. Reiss, "Absorption of Light by Light," J. Math. Phys. **3**, 59–67 (1962).

[13]V. P. Yakovlev, "Electron-positron pair production by a strong electromagnetic wave in the field of a nucleus," Sov. Phys. JETP **22**(1), 223–229 (1966), available at http://jetp.ras.ru/cgi-bin/dn/e_022_01_0223.pdf.

[14]K. Homma, K. Matsuura, and K. Nakajima, "Testing helicity-dependent $\gamma\gamma \rightarrow \gamma\gamma$ scattering in the region of MeV," Prog. Theor. Exp. Phys. **2016**, 013C01.

[15]C. Gahn, G. D. Tsakiris, G. Pretzler, K. J. Witte, C. Delfin, C. G. Wahlström, and D. Habs, "Generating positrons with femtosecond-laser pulses," Appl. Phys. Lett. **77**, 2662–2664 (2000).

[16]G. Sarri, K. Poder, J. M. Cole, W. Schumaker, A. Di Piazza, B. Reville, T. Dzelzainis, D. Doria, L. A. Gizzi, G. Grittani, S. Kar, C. H. Keitel, K. Krushelnick, S. Kuschel, S. P. D. Mangles, Z. Najmudin, N. Shukla, L. O. Silva, D. Symes, A. G. R. Thomas, M. Vargas, J. Vieira, and M. Zepf, "Generation of neutral and high-density electron–positron pair plasmas in the laboratory," Nat. Commun. **6**, 6747 (2015).

[17]D. Kolenatý, P. Hadjisolomou, R. Versaci, T. M. Jeong, P. Valenta, V. Olšovcová, and S. V. Bulanov, "Electron-positron pairs and radioactive nuclei production by irradiation of high-Z target with γ-photon flash generated by an ultra-intense laser in the λ^3 regime," Phys. Rev. Res. **4**, 023124 (2022).

[18]I. Pomerantz, E. McCary, A. R. Meadows, A. Arefiev, A. C. Bernstein, C. Chester, J. Cortez, M. E. Donovan, G. Dyer, E. W. Gaul, D. Hamilton, D. Kuk, A. C. Lestrade, C. Wang, T. Ditmire, and B. M. Hegelich, "Ultrashort pulsed neutron source," Phys. Rev. Lett. **113**, 184801 (2014).

[19]S. V. Bulanov, T. Z. Esirkepov, M. Kando, J. Koga, K. Kondo, and G. Korn, "On the problems of relativistic laboratory astrophysics and fundamental physics with super powerful lasers," Plasma Phys. Rep. **41**, 1–51 (2015).

[20]T. E. Cowan, A. W. Hunt, T. W. Phillips, S. C. Wilks, M. D. Perry, C. Brown, W. Fountain, S. Hatchett, J. Johnson, M. H. Key, T. Parnell, D. M. Pennington, R. A. Snavely, and Y. Takahashi, "Photonuclear fission from high energy electrons from ultraintense laser-solid interactions," Phys. Rev. Lett. **84**, 903–906 (2000).

[21]H. Schwoerer, F. Ewald, R. Sauerbrey, J. Galy, J. Magill, V. Rondinella, R. Schenkel, and T. Butz, "Fission of actinides using a tabletop laser," Europhys. Lett. **61**, 47–52 (2003).

[22]K. J. Weeks, V. N. Litvinenko, and J. M. Madey, "The Compton backscattering process and radiotherapy," Med. Phys. **24**, 417–423 (1997).

[23]C. M. Tarbert, D. P. Watts, D. I. Glazier, P. Aguar, J. Ahrens, J. R. M. Annand, H. J. Arends, R. Beck, V. Bekrenev, B. Boillat, A. Braghieri, D. Branford, W. J. Briscoe, J. Brudvik, S. Cherepnya, R. Codling, E. J. Downie, K. Foehl, P. Grabmayr, R. Gregor, E. Heid, D. Hornidge, O. Jahn, V. L. Kashevarov, A. Knezevic, R. Kondratiev, M. Korolija, M. Kotulla, D. Krambrich, B. Krusche, M. Lang, V. Lisin, K. Livingston, S. Lugert, I. J. D. MacGregor, D. M. Manley, M. Martinez, J. C. McGeorge, D. Mekterovic, V. Metag, B. M. K. Nefkens, A. Nikolaev, R. Novotny, R. O. Owens, P. Pedroni, A. Polonski, S. N. Prakhov, J. W. Price, G. Rosner, M. Rost, T. Rostomyan, S. Schadmand, S. Schumann, D. Sober, A. Starostin, I. Supek, A. Thomas, M. Unverzagt, T. Walcher, L. Zana, and F. Zehr, "Neutron skin of ^{208}Pb from coherent pion photoproduction," Phys. Rev. Lett. **112**, 242502 (2014).

[24]A. Ravasio, M. Koenig, S. Le-Pape, A. Benuzzi-Mounaix, H. S. Park, C. Cecchetti, P. Patel, A. Schiavi, N. Ozaki, A. Mackinnon, B. Loupias, D. Batani, T. Boehly, M. Borghesi, R. Dezulian, E. Henry, M. Notley, S. Bandyopadhyay, R. Clarke, and T. Vinci, "Hard x-ray radiography for density measurement in shock compressed matter," Phys. Plasmas **15**, 060701 (2008).

[25]L. Antonelli, S. Atzeni, A. Schiavi, S. D. Baton, E. Brambrink, M. Koenig, C. Rousseaux, M. Richetta, D. Batani, P. Forestier-Colleoni, E. Le Bel, Y. Maheut, T. Nguyen-Bui, X. Ribeyre, and J. Trela, "Laser-driven shock waves studied by x-ray radiography," Phys. Rev. E **95**, 063205 (2017).

[26]G. A. Mourou, T. Tajima, and S. V. Bulanov, "Optics in the relativistic regime," Rev. Mod. Phys. **78**, 309–371 (2006).

[27]J. Schwinger, "On gauge invariance and vacuum polarization," Phys. Rev. **82**, 664–679 (1951).

[28]S. V. Bulanov, T. Z. Esirkepov, Y. Hayashi, M. Kando, H. Kiriyama, J. K. Koga, K. Kondo, H. Kotaki, A. S. Pirozhkov, S. S. Bulanov, A. G. Zhidkov, P. Chen, D. Neely, Y. Kato, N. B. Narozhny, and G. Korn, "On the design of experiments for the study of extreme field limits in the interaction of laser with ultrarelativistic electron beam," Nucl. Instrum. Methods Phys. Res., Sect. A **660**, 31–42 (2011).

[29]L. D. Landau and E. M. Lifshitz, *The Classical Theory of Fields*, 4th rev.engl.ed., Course of Theoretical Physics – Pergamon International Library of Science, Technology, Engineering and Social Studies (Pergamon Press, Oxford, 1975).

[30]S. V. Bulanov, T. Z. Esirkepov, J. Koga, and T. Tajima, "Interaction of electromagnetic waves with plasma in the radiation-dominated regime," Plasma Phys. Rep. **30**, 196–213 (2004).

[31]F. Ehlotzky, K. Krajewska, and J. Z. Kamiński, "Fundamental processes of quantum electrodynamics in laser fields of relativistic power," Rep. Prog. Phys. **72**, 046401 (2009).

[32]I. V. Sokolov, J. A. Nees, V. P. Yanovsky, N. M. Naumova, and G. A. Mourou, "Emission and its back-reaction accompanying electron motion in relativistically strong and QED-strong pulsed laser fields," Phys. Rev. E **81**, 036412 (2010).

[33]C. P. Ridgers, C. S. Brady, R. Duclous, J. G. Kirk, K. Bennett, T. D. Arber, A. P. L. Robinson, and A. R. Bell, "Dense electron-positron plasmas and ultraintense γ rays from laser-irradiated solids," Phys. Rev. Lett. **108**, 165006 (2012).

[34]C. P. Ridgers, C. S. Brady, R. Duclous, J. G. Kirk, K. Bennett, T. D. Arber, and A. R. Bell, "Dense electron-positron plasmas and bursts of gamma-rays from

laser-generated quantum electrodynamic plasmas," Phys. Plasmas **20**, 056701 (2013).
[35]C. P. Ridgers, J. G. Kirk, R. Duclous, T. G. Blackburn, C. S. Brady, K. Bennett, T. D. Arber, and A. R. Bell, "Modelling gamma-ray photon emission and pair production in high-intensity laser–matter interactions," J. Comput. Phys **260**, 273–285 (2014).
[36]V. N. Baier, V. M. Katkov, and V. M. Strakhovenko, "Quantum radiation theory in inhomogeneous external fields," Nucl. Phys. B **328**, 387–405 (1989).
[37]V. Dinu, C. Harvey, A. Ilderton, M. Marklund, and G. Torgrimsson, "Quantum radiation reaction: From interference to incoherence," Phys. Rev. Lett. **116**, 044801 (2016).
[38]A. Di Piazza, M. Tamburini, S. Meuren, and C. H. Keitel, "Implementing nonlinear Compton scattering beyond the local-constant-field approximation," Phys. Rev. A **98**, 012134 (2018).
[39]A. Ilderton, "Note on the conjectured breakdown of QED perturbation theory in strong fields," Phys. Rev. D **99**, 085002 (2019).
[40]T. Heinzl, B. King, and A. J. MacLeod, "Locally monochromatic approximation to QED in intense laser fields," Phys. Rev. A **102**, 063110 (2020).
[41]R. A. Fonseca, L. O. Silva, F. S. Tsung, V. K. Decyk, W. Lu, C. Ren, W. B. Mori, S. Deng, S. Lee, T. Katsouleas, and J. C. Adam, "OSIRIS: A three-dimensional, fully relativistic particle in cell code for modeling plasma based accelerators," in *Computational Science—ICCS 2002*, edited by P. M. A. Sloot, A. G. Hoekstra, C. J. K. Tan, and J. J. Dongarra (Springer-Verlag, Berlin, Heidelberg, 2002), pp. 342–351.
[42]T. D. Arber, K. Bennett, C. S. Brady, A. Lawrence-Douglas, M. G. Ramsay, N. J. Sircombe, P. Gillies, R. G. Evans, H. Schmitz, and A. R. Bell, "Contemporary particle-in-cell approach to laser-plasma modelling," Plasma Phys. Controlled Fusion **57**, 113001 (2015).
[43]J. Derouillat, F. Beck, A. Pérez, T. Vinci, M. Chiaramello, A. Grassi, M. Flé, G. Bouchard, I. Plotnikov, N. Aunai, J. Dargent, C. Riconda, and M. Grech, "Smilei: A collaborative, open-source, multi-purpose particle-in-cell code for plasma simulation," Comput. Phys. Commun. **222**, 351–373 (2018).
[44]R. Duclous, J. G. Kirk, and A. R. Bell, "Monte Carlo calculations of pair production in high-intensity laser–plasma interactions," Plasma Phys. Controlled Fusion **53**, 015009 (2010).
[45]A. Rees, "EPOCH Bremsstrahlung routine," https://alun-rees.github.io/files/EPOCH_Bremsstrahlung_Routine.pdf (2019).
[46]B. Martinez, M. Lobet, R. Duclous, E. d'Humières, and L. Gremillet, "High-energy radiation and pair production by Coulomb processes in particle-in-cell simulations," Phys. Plasmas **26**, 103109 (2019).
[47]S. Morris, A. Robinson, and C. Ridgers, "Highly efficient conversion of laser energy to hard x-rays in high-intensity laser–solid simulations," Phys. Plasmas **28**, 103304 (2021).
[48]H. Chen, S. C. Wilks, J. D. Bonlie, E. P. Liang, J. Myatt, D. F. Price, D. D. Meyerhofer, and P. Beiersdorfer, "Relativistic positron creation using ultraintense short pulse lasers," Phys. Rev. Lett. **102**, 105001 (2009).
[49]A. R. Bell and J. G. Kirk, "Possibility of prolific pair production with high-power lasers," Phys. Rev. Lett. **101**, 200403 (2008).
[50]J. G. Kirk, A. R. Bell, and I. Arka, "Pair production in counter-propagating laser beams," Plasma Phys. Controlled Fusion **51**, 085008 (2009).
[51]F. Niel, C. Riconda, F. Amiranoff, R. Duclous, and M. Grech, "From quantum to classical modeling of radiation reaction: A focus on stochasticity effects," Phys. Rev. E **97**, 043209 (2018).
[52]P. Zhang, C. P. Ridgers, and A. G. R. Thomas, "The effect of nonlinear quantum electrodynamics on relativistic transparency and laser absorption in ultra-relativistic plasmas," New J. Phys. **17**, 043051 (2015).
[53]D. DelSorbo, D. R. Blackman, R. Capdessus, K. Small, C. Slade-Lowther, W. Luo, M. J. Duff, A. P. L. Robinson, P. McKenna, Z. M. Sheng, J. Pasley, and C. P. Ridgers, "Efficient ion acceleration and dense electron–positron plasma creation in ultra-high intensity laser-solid interactions," New J. Phys. **20**, 033014 (2018).
[54]C. M. Huntington, J. M. McNaney, E. Gumbrell, A. Krygier, C. Wehrenberg, and H.-S. Park, "Bremsstrahlung x-ray generation for high optical depth radiography applications on the National Ignition Facility," Rev. Sci. Instrum. **89**, 10G121 (2018).
[55]S. Palaniyappan, D. C. Gautier, B. J. Tobias, J. C. Fernandez, J. Mendez, T. Burris-Mog, C. K. Huang, A. Favalli, J. F. Hunter, M. E. Espy *et al.*, "MeV bremsstrahlung x rays from intense laser interaction with solid foils," Laser Part. Beams **36**, 502–506 (2018).
[56]A. Zhidkov, J. Koga, A. Sasaki, and M. Uesaka, "Radiation damping effects on the interaction of ultraintense laser pulses with an overdense plasma," Phys. Rev. Lett. **88**, 185002 (2002).
[57]T. Nakamura, J. K. Koga, T. Z. Esirkepov, M. Kando, G. Korn, and S. V. Bulanov, "High-power γ-ray flash generation in ultraintense laser-plasma interactions," Phys. Rev. Lett. **108**, 195001 (2012).
[58]K. V. Lezhnin, P. V. Sasorov, G. Korn, and S. V. Bulanov, "High power gamma flare generation in multi-petawatt laser interaction with tailored targets," Phys. Plasmas **25**, 123105 (2018).
[59]B. Martinez, E. d'Humières, and L. Gremillet, "Synchrotron radiation from ultrahigh-intensity laser-plasma interactions and competition with Bremsstrahlung in thin foil targets," Phys. Rev. Res. **2**, 043341 (2020).
[60]J. Vyskočil, E. Gelfer, and O. Klimo, "Inverse Compton scattering from solid targets irradiated by ultra-short laser pulses in the $10^{22} - 10^{23}$ W/cm^2 regime," Plasma Phys. Controlled Fusion **62**, 064002 (2020).
[61]L. L. Ji, A. Pukhov, I. Y. Kostyukov, B. F. Shen, and K. Akli, "Radiation-reaction trapping of electrons in extreme laser fields," Phys. Rev. Lett. **112**, 145003 (2014).
[62]M. J. Duff, R. Capdessus, D. DelSorbo, C. P. Ridgers, M. King, and P. McKenna, "Modelling the effects of the radiation reaction force on the interaction of thin foils with ultra-intense laser fields," Plasma Phys. Controlled Fusion **60**, 064006 (2018).
[63]S. V. Popruzhenko, T. V. Liseykina, and A. Macchi, "Efficiency of radiation friction losses in laser-driven 'hole boring' of dense targets," New J. Phys. **21**, 033009 (2019).
[64]D. J. Stark, T. Toncian, and A. V. Arefiev, "Enhanced multi-MeV photon emission by a laser-driven electron beam in a self-generated magnetic field," Phys. Rev. Lett. **116**, 185003 (2016).
[65]T. Wang, X. Ribeyre, Z. Gong, O. Jansen, E. d'Humières, D. Stutman, T. Toncian, and A. Arefiev, "Power scaling for collimated γ-ray beams generated by structured laser-irradiated targets and its application to two-photon pair production," Phys. Rev. Appl. **13**, 054024 (2020).
[66]H. G. Rinderknecht, T. Wang, A. Laso-Garcia, G. Bruhaug, M. S. Wei, H. J. Quevedo, T. Ditmire, J. Williams, A. Haid, D. Doria, K. M. Spohr, T. Toncian, and A. Arefiev, "Relativistically transparent magnetic filaments: Scaling laws, initial results and prospects for strong-field QED studies," New J. Phys. **23**, 095009 (2021).
[67]D. Younis, B. Hafizi, and D. F. Gordon, "Generation of collimated vortex gamma-rays from intense poincaré beam–plasma interaction," Phys. Plasmas **29**, 093106 (2022).
[68]W. M. Wang, Z. M. Sheng, P. Gibbon, L. M. Chen, Y. T. Li, and J. Zhang, "Collimated ultrabright gamma rays from electron wiggling along a petawatt laser-irradiated wire in the QED regime," Proc. Natl. Acad. Sci. **115**, 9911–9916 (2018).
[69]X. L. Zhu, M. Chen, S. M. Weng, T. P. Yu, F. Wang, W. M. He, Z. M. Sheng, P. McKenna, D. A. Jaroszynski, and J. Zhang, "Extremely brilliant GeV γ-rays from a two-stage laser-plasma accelerator," Sci. Adv. **6**, eaaz7240 (2020).
[70]H. Zhang, J. Zhao, Y. Hu, Q. Li, Y. Lu, Y. Cao, D. Zou, Z. Sheng, F. Pegoraro, P. McKenna *et al.*, "Efficient bright γ-ray vortex emission from a laser-illuminated light-fan-in-channel target," High Power Laser Sci. Eng. **9**, e43 (2021).
[71]S. Chintalwad, S. Krishnamurthy, B. Ramakrishna, and C. P. Ridgers, "Photon emission enhancement studies from the interaction of ultraintense laser pulses with shaped targets," Phys. Rev. E **105**, 025205 (2022).
[72]Y. J. Gu, O. Klimo, S. V. Bulanov, and S. Weber, "Brilliant gamma-ray beam and electron–positron pair production by enhanced attosecond pulses," Commun. Phys. **1**, 93 (2018).
[73]L. Zhang, S. Wu, H. Huang, H. Lan, W. Liu, Y. Wu, Y. Yang, Z. Zhao, Z. Zhu, and W. Luo, "Brilliant attosecond γ-ray emission and high-yield positron production from intense laser-irradiated nano-micro array," Phys. Plasmas **28**, 023110 (2021).
[74]I. P. Tsygvintsev and V. A. Gasilov, "On the density distribution of a plasma generated by a femtosecond laser prepulse," Math. Modell. **35**(1), 3–12 (2023) (in Russian).
[75]P. Hadjisolomou, T. M. Jeong, and S. V. Bulanov, "Towards bright gamma-ray flash generation from tailored target irradiated by multi-petawatt laser," Sci. Rep. **12**, 17143 (2022).

[76]W. Luo, Y.-B. Zhu, H.-B. Zhuo, Y.-Y. Ma, Y.-M. Song, Z.-C. Zhu, X.-D. Wang, X.-H. Li, I. C. E. Turcu, and M. Chen, "Dense electron-positron plasmas and gamma-ray bursts generation by counter-propagating quantum electrodynamics-strong laser interaction with solid targets," Phys. Plasmas **22**, 063112 (2015).
[77]T. Grismayer, M. Vranic, J. L. Martins, R. A. Fonseca, and L. O. Silva, "Laser absorption via quantum electrodynamics cascades in counter propagating laser pulses," Phys. Plasmas **23**, 056706 (2016).
[78]X. L. Zhu, T. P. Yu, Z. M. Sheng, Y. Yin, I. C. E. Turcu, and A. Pukhov, "Dense GeV electron–positron pairs generated by lasers in near-critical-density plasmas," Nat. Commun. **7**, 13686 (2016).
[79]X. L. Zhu, T. P. Yu, M. Chen, S. M. Weng, and Z. M. Sheng, "Generation of GeV positron and γ-photon beams with controllable angular momentum by intense lasers," New J. Phys. **20**, 083013 (2018).
[80]M. Vranic, T. Grismayer, R. A. Fonseca, and L. O-Silva, "Electron–positron cascades in multiple-laser optical traps," Plasma Phys. Controlled Fusion **59**, 014040 (2016).
[81]W. Luo, W. Y. Liu, T. Yuan, M. Chen, J. Y. Yu, F. Y. Li, D. Del Sorbo, C. P. Ridgers, and Z. M. Sheng, "QED cascade saturation in extreme high fields," Sci. Rep. **8**, 8400 (2018).
[82]C. Slade-Lowther, D. Del Sorbo, and C. P. Ridgers, "Identifying the electron–positron cascade regimes in high-intensity laser-matter interactions," New J. Phys. **21**, 013028 (2019).
[83]Z. Gong, R. H. Hu, Y. R. Shou, B. Qiao, C. E. Chen, X. T. He, S. S. Bulanov, T. Z. Esirkepov, S. V. Bulanov, and X. Q. Yan, "High-efficiency γ-ray flash generation via multiple-laser scattering in ponderomotive potential well," Phys. Rev. E **95**, 013210 (2017).
[84]H.-Z. Li, T.-P. Yu, J.-J. Liu, Y. Yin, X.-L. Zhu, R. Capdessus, F. Pegoraro, Z.-M. Sheng, P. McKenna, and F.-Q. Shao, "Ultra-bright γ-ray emission and dense positron production from two laser-driven colliding foils," Sci. Rep. **7**, 17312 (2017).
[85]N. Yasen, B. Xie, and W. Liu, "Dense positrons and γ-rays generation by lasers interacting with convex target," Plasma Sci. Technol. **23**, 015003 (2020).
[86]P. Hadjisolomou, T. M. Jeong, P. Valenta, D. Kolenaty, R. Versaci, V. Olšovcová, C. P. Ridgers, and S. V. Bulanov, "Gamma-ray flash in the interaction of a tightly focused single-cycle ultra-intense laser pulse with a solid target," J. Plasma Phys. **88**, 905880104 (2022).
[87]T. M. Jeong, S. V. Bulanov, P. V. Sasorov, S. S. Bulanov, J. K. Koga, and G. Korn, "4π-spherically focused electromagnetic wave: Diffraction optics approach and high-power limits," Opt. Express **28**, 13991–14006 (2020).
[88]G. Mourou, Z. Chang, A. Maksimchuk, J. Nees, S. V. Bulanov, V. Y. Bychenkov, T. Z. Esirkepov, N. M. Naumova, F. Pegoraro, and H. Ruhl, "On the design of experiments for the study of relativistic nonlinear optics in the limit of single-cycle pulse duration and single-wavelength spot size," Plasma Phys. Rep. **28**, 12–27 (2002).
[89]P. Hadjisolomou, T. M. Jeong, P. Valenta, G. Korn, and S. V. Bulanov, "Gamma-ray flash generation in irradiating a thin foil target by a single-cycle tightly focused extreme power laser pulse," Phys. Rev. E **104**, 015203 (2021).
[90]V. A. Vshivkov, N. M. Naumova, F. Pegoraro, and S. V. Bulanov, "Nonlinear electrodynamics of the interaction of ultra-intense laser pulses with a thin foil," Phys. Plasmas **5**, 2727–2741 (1998).
[91]T. M. Jeong, S. V. Bulanov, S. Weber, and G. Korn, "Analysis on the longitudinal field strength formed by tightly-focused radially-polarized femtosecond petawatt laser pulse," Opt. Express **26**, 33091–33107 (2018).
[92]C. Ahdida, D. Bozzato, D. Calzolari, F. Cerutti, N. Charitonidis, A. Cimmino, A. Coronetti, D. D'alessandro, A. Donadon-Servelle, L. Esposito, R. Froeschl, R. G. Alía, A. Gerbershagen, S. Gilardoni, D. Horváth, G. Hugo, A. Infantino, V. Kouskoura, A. Lechner, and B. Lefebvre, "New capabilities of the FLUKA multi-purpose code," Front. Phys. **9**, 788253 (2022).
[93]G. Battistoni, T. Boehlen, F. Cerutti, P. W. Chin, L. S. Esposito, A. Fassò, A. Ferrari, A. Lechner, A. Empl, A. Mairani, P. G. Mereghetti, A. Ortega, J. Ranft, S. Roesler, P. R. Sala, V. Vlachoudis, and G. Smirnov, "Overview of the FLUKA code," Ann. Nucl. Energy **82**, 10–18 (2015).
[94]S. C. Vogel, J. C. Fernandez, D. C. Gautier, N. Mitura, M. Roth, and K. F. Schoenberg, "Short-pulse laser-driven moderated neutron source," EPJ Web Conf. **231**, 01008 (2020).
[95]D. P. Higginson, J. M. McNaney, D. C. Swift, T. Bartal, D. S. Hey, R. Kodama, S. L. Pape, A. Mackinnon, D. Mariscal, H. Nakamura, N. Nakanii, K. A. Tanaka, and F. N. Beg, "Laser generated neutron source for neutron resonance spectroscopy," Phys. Plasmas **17**, 100701 (2010).
[96]M. Zimmer, S. Scheuren, A. Kleinschmidt, A. Tebartz, T. Ebert, J. Ding, D. Hartnagel, and M. Roth, "Development of a setup for material identification based on laser-driven neutron resonance spectroscopy," EPJ Web Conf. **231**, 01006 (2020).
[97]J. P. evol, "An accelerator-driven system for the destruction of nuclear waste," Prog. Nucl. Energy **38**, 153–166 (2001).
[98]A. Azzam, S. A. Said, and M. Al-abyad, "Evaluation of different production routes for the radio medical isotope 203Pb using TALYS 1.4 and EMPIRE 3.1 code calculations," Appl. Radiat. Isot. **91**, 109–113 (2014).
[99]E. Tadamura, T. Kudoh, M. Motooka, M. Inubushi, S. Shirakawa, N. Hattori, T. Okada, T. Matsuda, T. Koshiji, K. Nishimura, K. Matsuda, and J. Konishi, "Assessment of regional and global left ventricular function by reinjection Tl-201 and rest Tc-99m sestamibi ECG-gated SPECT: Comparison with three-dimensional magnetic resonance imaging," J. Am. Coll. Cardiol. **33**, 991–997 (1999).
[100]A. Fedotov, A. Ilderton, F. Karbstein, B. King, D. Seipt, H. Taya, and G. Torgrimsson, "Advances in QED with intense background fields," Phys. Rep. **1010**, 1–138 (2023).
[101]A. J. MacLeod, P. Hadjisolomou, T. M. Jeong, and S. V. Bulanov, "All-optical nonlinear Breit-Wheeler pair production with γ-flash photons," Phys. Rev. A **107**, 012215 (2023).
[102]A. Golub, S. Villalba-Chávez, and C. Müller, "Nonlinear Breit-Wheeler pair production in collisions of bremsstrahlung γ quanta and a tightly focused laser pulse," Phys. Rev. D **105**, 116016 (2022).
[103]A. Di Piazza, C. Müller, K. Z. Hatsagortsyan, and C. H. Keitel, "Extremely high-intensity laser interactions with fundamental quantum systems," Rev. Mod. Phys. **84**, 1177–1228 (2012).
[104]P. Zhang, S. S. Bulanov, D. Seipt, A. V. Arefiev, and A. G. R. Thomas, "Relativistic plasma physics in supercritical fields," Phys. Plasmas **27**, 050601 (2020).
[105]A. Gonoskov, T. G. Blackburn, M. Marklund, and S. S. Bulanov, "Charged particle motion and radiation in strong electromagnetic fields," Rev. Mod. Phys. **94**, 045001 (2022).